The role of density gradients on tidal asymmetries in the German Bight

**Emil V. Stanev · Rahma Al-Nadhairi ·
Arnoldo Valle-Levinson**

Abstract The dynamics of the German Bight associated with river plumes and fresh water intrusions from tidal flats have been studied with numerical simulations. The horizontal and vertical patterns of the M_2, M_4 and M_6 tides revealed complex distortions along the bathymetric channels connecting the coast and the open sea. A major focus was on the surface-to-bottom change in tidal asymmetries, which provides a major control on draining the tidal flats around the Elbe and Weser River mouths. Comparisons between baroclinic and barotropic experiments demonstrated that the estuarine gravitational circulation is responsible for pronounced differences in surface and bottom asymmetries. These differences could be considered as a basic control mechanism for sediment dynamics. The most prominent area of tidal distortions, manifested by a delay of the tidal wave, was located between the estuarine turbidity maximum and the estuarine mouth north of Cuxhaven. This area was characterized by the strongest periodic convergence and divergence of the flow and by the largest salinity gradients. The enhancement of the gravitational circulation occurred during the transition between spring and neap tides. The large-scale dynamics and small-scale topographic features could impact the sediment distribution as there was a marked interplay in the channels between stratification and turbulence. Also an explanation has been given for the mechanisms supporting the existence of a mud area (*Schlickgebiet*) south of Helgoland Island, associated with trapping suspended particular matter.

E. V. Stanev (✉) · R. Al-Nadhairi
Helmholtz-Zentrum Geesthacht, 21502 Geesthacht, Germany
e-mail: emil.stanev@hzg.de

A. Valle-Levinson
University of Florida, Gainesville, FL 32611, USA

1 Introduction

Flood and ebb tidal transports in coastal areas determine the dispersion and mixing of fresh water plumes and provide a major link between terrestrial and marine systems. These transports, which can be either vertically sheared or uniform, are characterized by complex interactions of processes at multiple temporal and spatial scales. In the German Bight (Fig. 1a), nonlinear tidal distortions largely modify the tide spectrum of the incoming Kelvin wave (Stanev et al. 2014). This leads to asymmetries affecting the transport and exchange of matter between the coastal zone and the open ocean. Additionally, the bathymetric channels in the German Bight act as major transport avenues connecting the tidal flats and the open ocean. However, their role in the regional hydro-and-sediment dynamics is still not fully understood. Regional asymmetries of tidal oscillations have been largely associated with the complex bathymetry (Stanev et al. 2014). The present work continues the research on the role of water density in the German Bight (e.g. Backhaus 1980) focussing on the intrusion of open ocean water into the coastal zone and the export of mixed river water into the open ocean. The resulting spatial changes of the spectral composition in the tidal signal may explain the local sediment accumulation patterns in the study area.

As demonstrated by Backhaus (1980), the sense of rotation of tidal currents in the German Bight and Elbe Estuary changes in space and as a function of depth. His numerical study supported observations revealing that the sense of rotation of surface currents is not representative for the entire water column in some areas. One factor that explained the spatial variability of the sense of rotation of tidal ellipses was the role

of stratification (see also Stanev et al. 2014). This explanation was consistent with the rotation changing from counterclockwise over most of the German Bight to clockwise in the Elbe Estuary (Sager 1968). However, according to Backhaus, the change of rotation with increasing depth could also appear in a homogeneous ocean. Although this fundamental property of tidal currents is relevant to almost all aspects of coastal tidal dynamics under fresh water influence, its temporal and spatial variability is still not well understood in the German Bight, which is the area of this study. However, this scarcity of understanding is apparent in other regions. In the present study, such paucity will be addressed by investigating the spectral composition of tides in the coastal ocean.

An overall motivation for the present study is to describe some of the physical mechanisms in the German Bight that could be responsible for the dominant features in the sediment distribution. This approach (to analyse physics with the aim to understand sediment dynamics) follows that of Postma (1961), Groen (1967), and Friedrichs and Aubrey (1988), who revealed the impact of tidal asymmetries on sediment transport. Later, Ridderinkhof (1997) showed that the direction of the net transport depended mainly on the phase difference between M_4 and M_2. Thus, the net sediment transport was ebb- or flood dominated in cases of short ebb or flood, respectively. The latter study, as well as those by van de Kreeke and Robaczewska (1993) and van Leeuwen and de Swart (2002), developed a theoretical understanding based on examples of several individual estuaries dominated by similar physical mechanisms (e.g. see Hansen and Rattray 1966 and Valle-Levinson 2010, 2011). However, less is known just outside the estuaries, i.e. at the region linking estuaries with the open ocean. Recently, it has been demonstrated by Stanev et al. (2014) that the simulated patterns of tidal signals in the German Bight correlate well with the observed distribution of bottom sediment size. This explained the importance of tidal distortion on sediment dynamics and gave confidence in the results of a 3D numerical model to address related sediment studies.

The hydrodynamics and sediment dynamics in the eastern part of the German Bight have been previously studied in relatively small areas. Stanev et al. (2007a) focused only on the well-mixed East Frisian Wadden Sea demonstrating the differences between sediment transport in the tidal flats, deep inlets and open sea. Rolinski and Eichweber (2000) demonstrated that the tidal wave transformations in the Elbe Estuary, combined with salinity gradients and residual currents, gave rise to estuarine turbidity maxima (ETM). The positions of ETM zones in the Weser and Elbe Rivers are shown in Fig. 1b (see for more details Kappenberg and Fanger 2007 and Kappenberg and Grabemann 2001). At the North Sea scales, the impact of stratification conditions on currents and their spectra has been studied by Backhaus (1980) and van Haren (2003). Carbajal and Pohlmann (2004) showed that baroclinic

effects significantly modify the inclination of tidal ellipses. However that study, because of the relatively coarse horizontal resolution used, did not address the effects of baroclinicity in the river mouths.

The Wadden Sea and the estuaries in the German Bight are characterized by Suspended Particular Matter (SPM) concentrations between 4 mg/l in summer and 18.5 mg/l in winter. This area thus represents an important (regional) element of the sedimentary system: *the source area*. Another important element of the sediment distributions in the German Bight is the so-called mud area (*Schlickgebiet*) south of the Helgoland Island and offshore of the Elbe and Weser Estuaries (see the white contour line in Fig. 1b). This is an approximately 500-
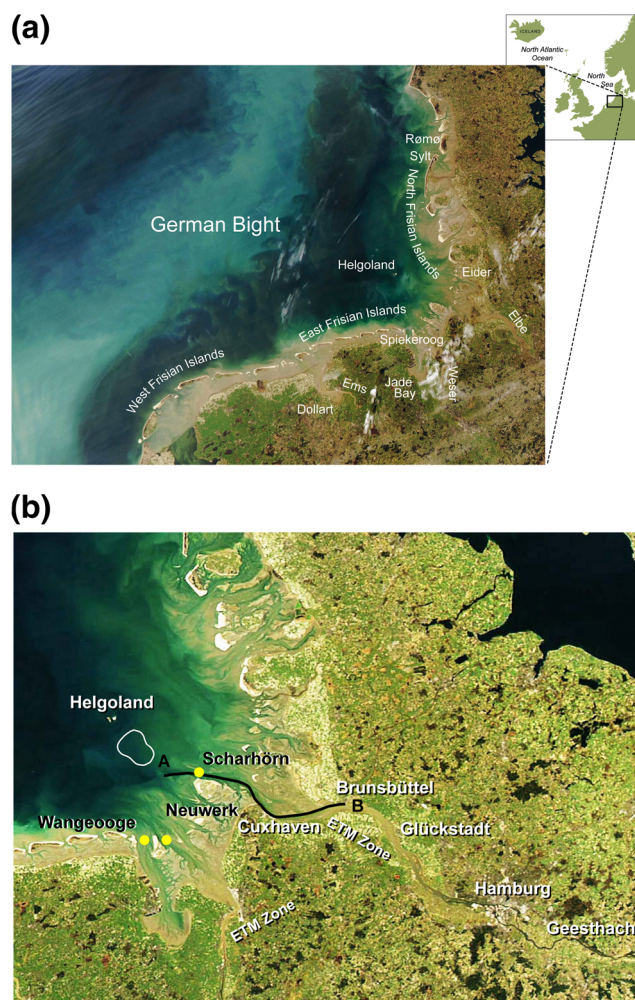
(a)

(b)

Fig. 1 **a** North Sea and German Bight. The image is of Aqua/MODIS March 9, 2014, 11:50 UTC showing the sediment in the North Sea (the North-Frisian front is well seen). Some geographical names used in the text are added. **b** Same but for March 12, 2014, 12:20 UTC in the estuarine region. Along-channel section where analysis of numerical simulations are presented in the text is identified on the map by lines *A–B*. The *yellow dots* display the locations where model data are also analysed. The *white line* gives the approximate contours of Helgoland mud area (Helgoländer Schlickgebiet) represented by the 20-m mud-thickness line (from von Haugwitz et al. 1988). The approximate locations of the ETM zones in the Elbe and Weser estuaries are also given

km² area, between the 15 m isobath in its eastern part and the 40 m isobath to the west (Figge 1981; Mayer 1995), where the thickness of the mud layer reaches 29 m. One could then speculate that *this mud area* is representative for the sink of fine sediment. The *Schlickgebiet* was created during the Holocene, and the modern sedimentation there is also quite substantial (about 1 to 10 mm/year). However, an explanation of the hydrodynamics maintaining the stability of *Schlickgebiet* is still missing. *Another suspended sediment area*, which is between the source and the sink (the ETM and Wadden Sea, from one side and the *Schlickgebiet*, from the other) can be considered as the transition zone. This ≈30–40-km wide coastal zone, which is well noticeable on satellite images (Fig. 1b), is of crucial importance for the exchange of sediment between the estuaries and the open ocean. It is likely that the bathymetric channels guide the exchange of sediment between the source (Wadden Sea) and the sink (*Schlickgebiet*). However, the transport processes in this region have not been quantified in detail, which motivated this study. The main objectives were to (1) carry out an analysis of the hydrodynamics in the area between the estuarine mouths and the open sea and (2) focus on the vertical properties of tidal distortion associated with density stratification, which was not addressed in the study of Stanev et al. (2014).

The paper has been structured as follows: Section 2 presents the numerical model and experiments; the overall characteristics of the tidal dynamics are presented in Section 3; Section 4 describes the role of density; Sections 5 and 6 address the horizontal and vertical patterns of tidal asymmetries, followed by discussion and conclusions.

2 The numerical model

The General Estuarine Transport Model (GETM, Burchard and Bolding 2002) was used in this study. This model solves the primitive equations for momentum, temperature, salinity and sea level. It uses the k-ε turbulence closure parameterization to solve for the turbulent kinetic energy (TKE) k and its dissipation rate ε. The model accounts for flooding and drying, which are relevant processes in the Wadden Sea (Stanev et al. 2003).

Three one-way nested setups were used: (1) a coarse-resolution North Sea–Baltic Sea model with 3 NM horizontal resolution (see Figure 6 of Stanev et al. 2011), (2) an intermediate-resolution (1 km) German Bight model, and (3) a fine-resolution (400 m) model for the south-eastern corner of German Bight (Fig. 2). The three models have the same vertical resolution of 21 σ-layers. The sea surface elevation at the open boundary of the North Sea–Baltic Sea model was generated using 13 tidal constituents obtained from satellite altimeter data via the OSU Tidal Inversion Software (Egbert and Erofeeva 2002). More details about the forcing at the open

boundary are given by Stanev et al. (2014). The three models were forced by atmospheric fluxes computed from bulk aerodynamic formulas using model-simulated sea surface temperature and data from the atmospheric analyses: 2 m temperature and relative humidity and 10 m wind, as well as cloud cover and precipitation. This atmospheric information originated from the regional model COSMO-EU, operated by the German Weather Service with a horizontal resolution of 7 km. Hourly river run-off data were provided by the German Federal Maritime and Hydrographic Agency (Bundesamt für Seeschifffahrt und Hydrographie, BSH). Temperature and salinity boundary conditions at the open boundaries of the North Sea–Baltic Sea model were interpolated from monthly mean climatological data at each time step.

The intermediate-resolution model (the model area is shown in Fig. 2a) was nested in the coarser domain model as explained by Staneva et al.(2009). The open boundary conditions were provided from the North Sea–Baltic Sea model. The fine-resolution estuarine model (Fig. 2b) was nested in the German Bight model (see the red box in Fig. 2a). The open boundary conditions were provided from the German Bight model. The network of multiple channels with an average channel depth of ≈20 m is well resolved in the estuarine model (Fig. 2b). To the west of the Elbe Estuary, the Weser Estuary and the Jade Channel are the most pronounced
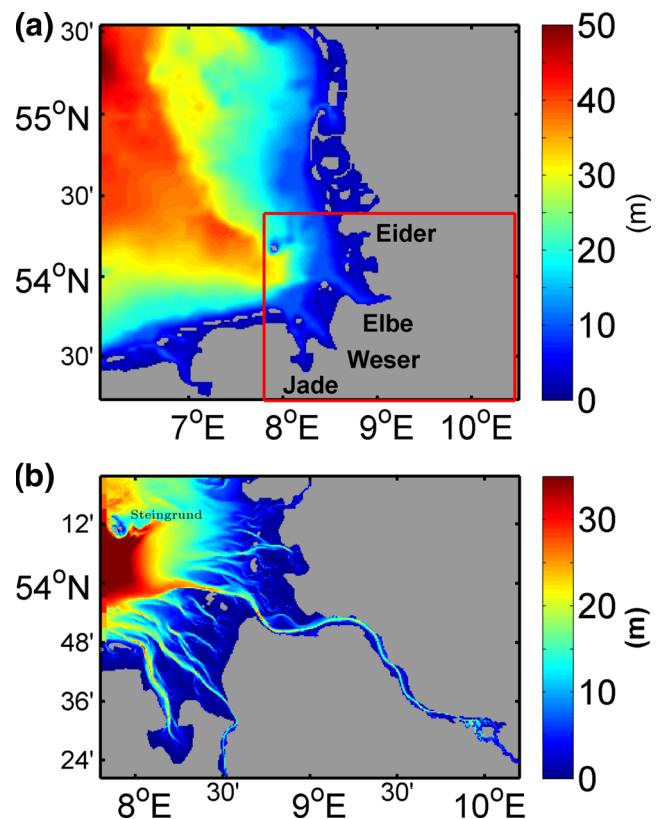

Fig. 2 **a** Bathymetry of the German Bight (in m) as used in the 1-km resolution model. **b** Same but only for the south-eastern part resolved with a horizontal grid of 400 m (*red box* in (a))

coastal and topographic features (see Figs. 1a and 2a for the geographic locations). The bathymetry of these estuarine extensions is also very complex, as seen in Fig. 3 for the Elbe Channel plotted along the section line in Fig. 1b.

The performance of the nested models and some comparisons with observations has been addressed by Stanev et al. (2014). This study demonstrated that the amplitude of M_2 tide increased continuously from the open sea toward the German Bight corner triggering a chain of important transformations of tide spectrum. The change of M_2 tide and the generation of overtides in the coastal ocean were dominated by mesoscale dynamics and bathymetric channels.

The results from the tidal analysis (Pawlowicz et al. 2002) of the model output for 28 days during May 2011 are discussed in the following with the aim to illustrate and quantify the distortion of tides associated with water column stratification. This period was chosen because of the relative calm atmospheric conditions, which enabled to reveal the role of tides under stratified conditions.

3 The estuarine circulation in the German bight: an overall presentation

3.1 Vertical structure of flows and salinity

The estuarine circulation (Geyer and MacCready 2014) is a bidirectional (exchange) flow, which forms under the inflow of rivers. Tidal forcing enhances the vertical mixing, distributing the buoyancy in the water column. Of utmost importance here is the sensitivity of mixing to the effect of stratification (large vertical turbulent exchange in the unstratified flows and weak within the stratified pycnocline). The
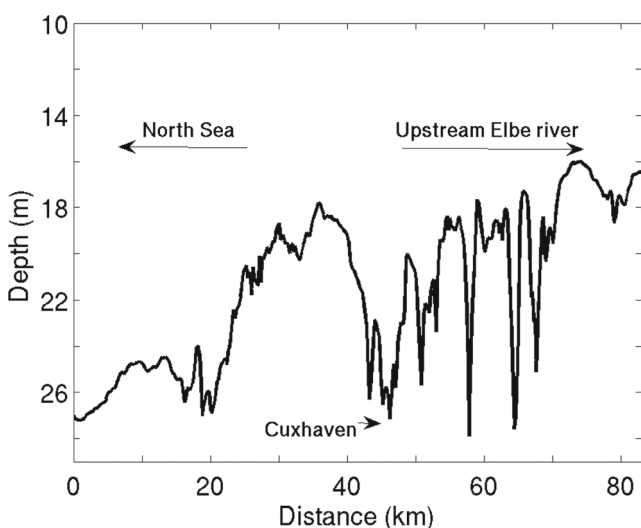

Fig. 3 Along-channel topography. The position of the channel is shown with the *thick black line* in Fig. 1b. The distance in kilometres is measured from the westernmost part of the section line

interactive coupling between all mechanisms results in a specific vertical stratification. The mean situation displays a two-layer flow with low-salinity water propagating seaward in the surface layers and ocean water flow in the bottom layer propagating in the opposite direction. The ensuing text describes how this general concept applies to bathymetric channels. An example is given for the transect line in Fig. 1b (for the bottom topography along this line see Fig. 3), which follows the thalweg of the Elbe River.

The basic tidal variations along the bathymetric channel are displayed in Fig. 4 by the back-and-forth oscillation of the front between km 30 and 50 off of Cuxhaven (~km 46, see Figs. 2b and 3). The position and sharpness of the front change dramatically between flood (Fig. 4a) and ebb (Fig. 4c). During ebb, the low-salinity surface water penetrates deeper into the open ocean, while during flood it is displaced up the channel and shrinks in the area of Cuxhaven. The front is nearly depth-independent in almost the whole water column (except for the top 3–4 m). Several zones of increased horizontal gradients can be identified, which appear and disappear during different phases of the tide.

The velocity vectors in Fig. 4 give a clear indication about the phase shifts of the current along the channel. While in the open ocean the ebb flow dominates the flow pattern in Fig. 4b, east of Cuxhaven, the flow is still directed up-river, i.e. a strong divergence occurs at about km 45. About 6 h later (Fig. 4e), a convergent flow develops almost in the same position that is seaward of Cuxhaven. Two hours earlier before the occurrence of maximum divergence/convergence (Fig. 4a, d, respectively), similar zones were observed at the beginning of the cross section (around location "A" in Fig. 1b). The analysis of co-phase lines provided by Stanev et al. (2014) demonstrated that there was a marked delay in the tidal wave propagating along the Elbe River between Cuxhaven and the area of bifurcation of the Elbe Channel. This delay was about two times larger than the delay in the open ocean measured for the same distance.

It is noteworthy that the zone of maximum along-channel salinity gradient at about km 40–50 coincides with the absolute maximum in flow divergence/convergence. It will be demonstrated later in this study that the dynamics of a salinity front is closely related to the nonlinear tidal transformations there. This could affect regional morphodynamics, in particular, the migration of channels (Winter et al. 2011) and bifurcation of the Elbe channel on both sides of the large bank north of Cuxhaven (see also Fig. 2b).

3.2 Vertical profiles

The typical vertical profiles of salinity and horizontal velocity (Fig. 5a, b) are analysed below in the channels connecting Jade Bay, Weser and Elbe mouths with the open sea (see yellow circles in Fig. 1b for the respective locations). The overall

Fig. 4 Vertical section of salinity with velocity (u, w) overimposed along the channel line in Fig. 1b. The timing of individual plots (**a–f**) differs in time steps by 2 h
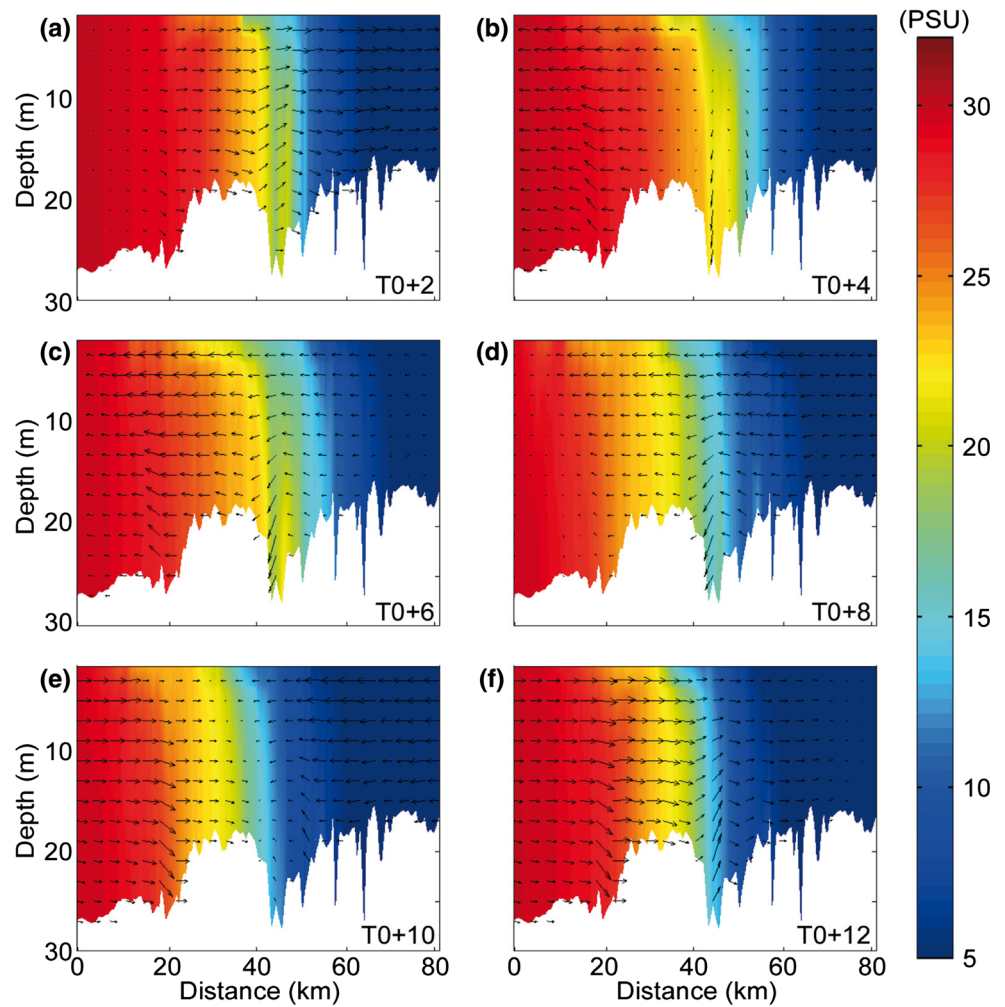
purpose here is to show (1) the estuarine circulation and (2) its rather different appearance in the three channels. In Jade Bay, the fresh water flux was almost negligible and salinity stratification was weak (black profiles in Fig. 5a remained vertical during flood and ebb) with salinity decreasing by about 2 g/kg from flood to ebb. The vertical stratification in the Weser channel was also weak during flood, like in the neighbouring Jade Channel. The flood to ebb differences reached about 3 g/kg at sea surface; the vertical gradients were quite pronounced during ebb reaching 2 g/kg between 4 and 12 m. The situation in the Elbe channel was different from the previous two. There, the bottom layer (from 17 to 22 m) was stratified during flood because of the intrusion of high-salinity ocean water. The surface-to-bottom salinity increase of about 1.5 g/kg during ebb was almost linearly distributed over the upper 19 m.

The vertical shear of horizontal tidal velocities displayed the well-known influence of tidal asymmetries on turbulence (Jay and Smith 1990). The largest velocity amplitude was in the Jade Bay channel because of the largest tidal prism of the area. The flood shear was largest in the Elbe bathymetric channel, while in the same location and at depths of about

8 m, the ebb flow showed a sub-surface velocity maximum. Tidal oscillations had the lowest amplitudes in the Weser channel, in particular, in the bottom layer.

In the case of estuarine circulation, the density-driven flow reverses with depth. In the locations considered in Fig. 5c, the specific distribution of salinity and velocity resulted in a two-layer pattern of the time-averaged transport of salt. In the Jade Bay channel, the upper layer displayed a very weak transport in the ebb direction, while in the deeper layers, salt transport was in the flood direction. The direction of the salt transport in the Elbe and Weser bathymetric channels obeyed similar overall distribution as in the Jade Bay channel; however, the vertical shear was much more pronounced. The transport in the Weser surface layer showed a maximum at about 1.5 g/kg*m/s. The decrease of salt transport above this depth was explained as a consequence of tidally induced Stokes drift (Stanev et al. 2007b). The vertical profile in the two channels appeared geometrically similar; however, the transports in Weser Bay were relatively much smaller. The reversal depth was shallower in the Weser channel, as well as the depth of maximum flood-directed (in deep layers) salt transport.
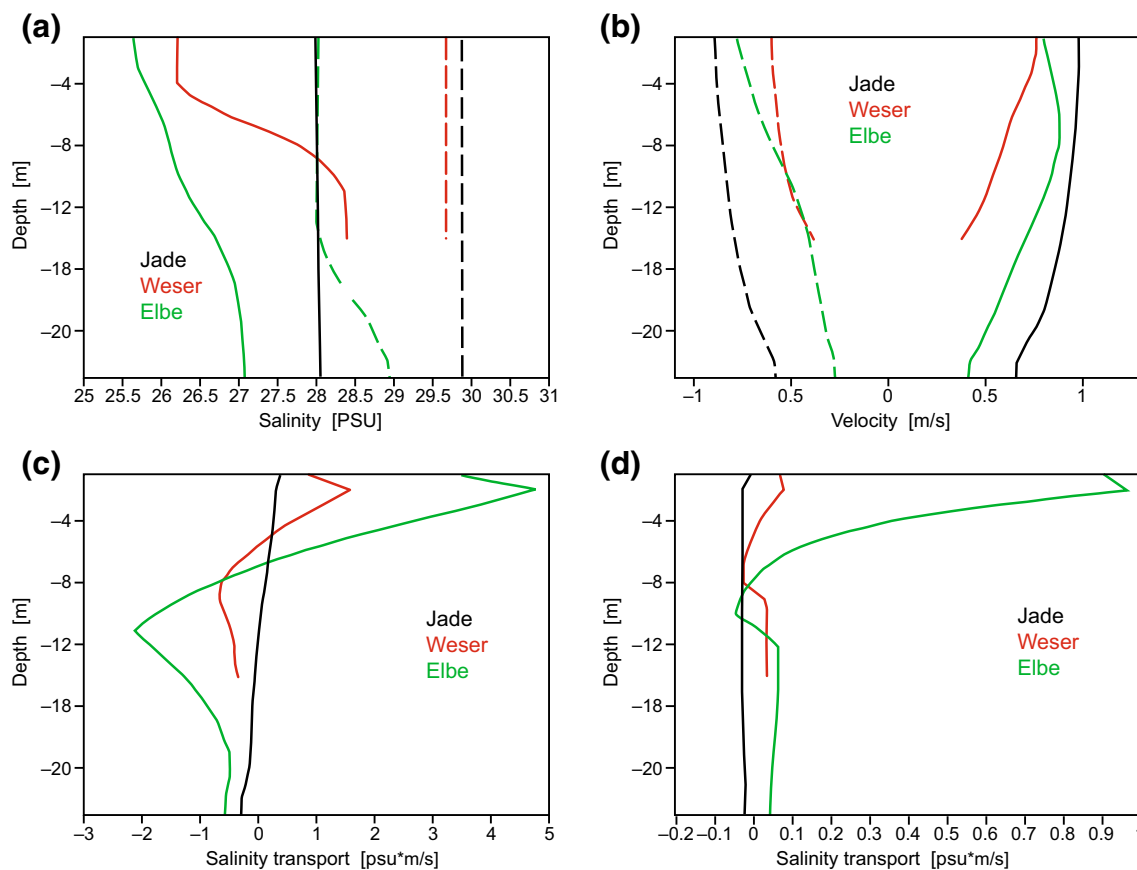
Fig. 5 Vertical profiles of salinity (**a**), velocity (**b**), salt transport (**c**) and nonlinear contribution to advection (**d**). The positions of chosen locations are shown in Fig. 1b with the *yellow symbols*. *Dash* and *full lines* correspond to flood and ebb situations

The existence of flood-directed maximum of salt transport $\{uS\}$ with a core which was relatively high above the bottom poses the question of whether it was due to the specific mean profiles $\{u\}$ $\{S\}$ or to the contribution of correlation between salinity and velocity at intra-tidal time scales $\{u'S'\}$, where $\{.\}$ is the temporal mean. Figure 5d made clear that about 20 % of the salt transport was explained by the correlation term, and this can be considered as a measure of the along-channel diffusivity due to tidal correlation of velocity and salinity (Geyer and MacCready 2014). This term approximately repeated the shape of the total transport in Elbe and Weser channels. In other words, the correlation between salinity and velocity tended to enhance the vertical overturning in the water column. In the rather barotropic channel of Jade Bay, the correlation between salinity and velocity tended to enhance the flood-oriented salt transport in the entire water column.

4 Regions of fresh water influence

The tidal mixing in the German Bight reduces largely the vertical gradients caused by the river flows, at the same time it enhances the horizontal gradients in the whole water column

(see Fig. 4). One way to quantify the effects from the river flows is to analyse the differences between the variables simulated in the barotropic and baroclinic experiments. A similar analysis was carried out in the past by Backhaus (1980) who studied the change of the sense of rotation of tidal currents in the German Bight and Elbe Estuary in space and as a function of depth. In the following, we will focus on the sea level as an adequate "integrator" of dominant processes.

The numerical simulations described in Section 2, to which we will refer to as control run (CR), were repeated as barotropic run (BR) by keeping the temperature and salinity constant. Thus, the density-driven contribution was removed in the BR. The river run-off was not switched off in the BR to minimize changes between the two experiments as this concerns the balance between barotropic pressure gradient and friction in the river head (Geesthact weir, Fig. 1a). The differences between the baroclinic and barotropic cases illustrated by the distributions of sea level differences during different phases of tide in Fig. 6 identified clearly the fresh water influence in the region. These differences were essentially caused by the Elbe and Weser estuaries. The sea level for the Elbe River was more than 15 cm higher in CR than in BR. Jade Bay, in contrast, remained almost insensitive to baroclinicity because of the missing fresh water sources there.

Fig. 6 Difference in surface elevation simulated in baroclinic and barotropic experiments during flood (2011/04/19/T01:00) (**a**), slack flood (2011/04/19T04:00) (**b**), ebb (2011/04/19/T07:00) (**c**) and slack ebb (2011/04/19T10:00) (**d**)
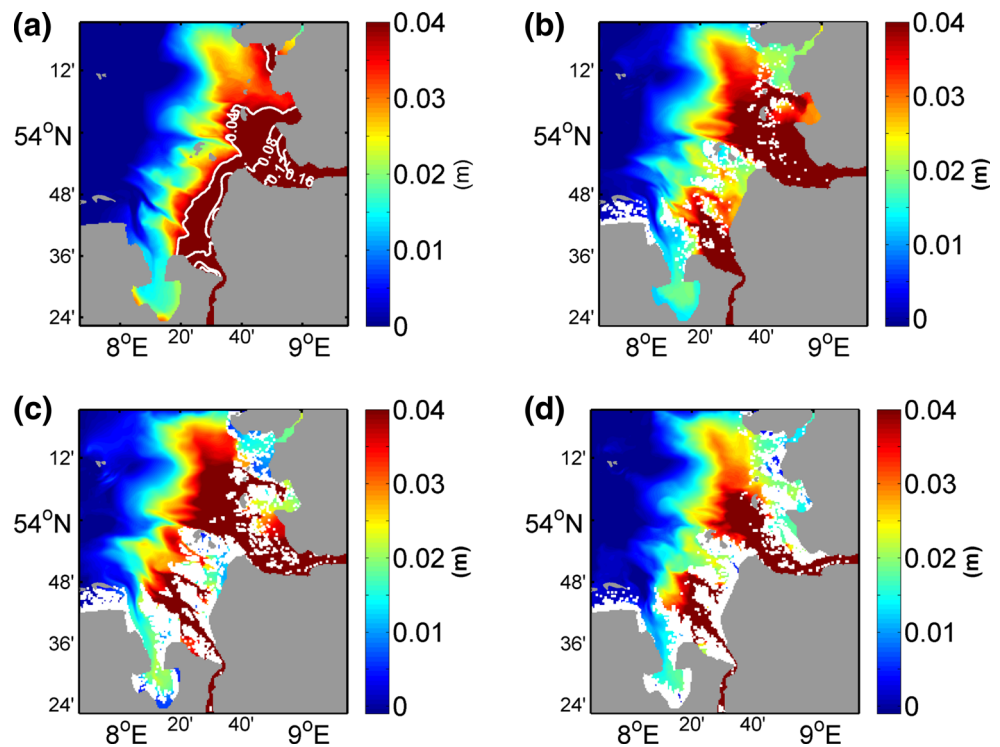
The difference between the sea level in BR and CR was about 2 mm/km, which would correspond to a geostrophic current of about 20 cm/s. The change of steric anomalies in the upper 15–20 m of river plumes simulated in CR ranged up to several centimetres, showing a clear response to atmospheric forcing with tidal oscillations superimposed. The corresponding ranges in the open sea were negligible. The large difference between the steric heights in the coastal and open sea areas and the large variability of the former manifested the dynamic impact of tidal excursions and transport of low-salinity water in the regions of fresh water influence (ROFIs).

The differences in the simulated BR and CR water level changed with tidal phase (compare individual fields during flood, end of flood, ebb and end of ebb). Some of the horizontal patterns were associated with bathymetric features. The plume of the Elbe River distinguished in the water-level difference map remained separated from the Weser River plume during most of the tidal cycle. This was just a demonstration that the ebb transport could not cross the tidal flats separating the two plumes. The plumes merged only during flood in front of Cuxhaven.

TKE was analysed in order to assess the dynamic consequences of nonuniform density fields and their possible impact on the sediment dynamics. The basic concept here is that stratification influences the production of TKE, thus the comparison between simulations in CR and BR would reveal the associated changes in the strength of turbulence. Figure 7 displays the differences in bottom TKE caused by baroclinicity. Because the bed shear stress controls the

deposition and remobilization of sediment, the differences between the two simulations are indicative of the possible change of sediment dynamics caused by the density field. Overall, the stratification caused by the river fluxes tends to decrease TKE, as expected. There were, however, two features to note in the horizontal patterns. The first one was illustrated by the reduced TKE values in the channels of Elbe and Weser, which were better seen during the end of flood and end of ebb. This would suggest that vertical stratification decreased the bottom erosion in the tidal channels. The second feature was the reduced TKE in the area of the *Schlickgebiet*. The latter would mean that baroclinicity enhanced deposition in that area (and suppress remobilization), which proposed a mechanism for trapping sediment in this region. One can thus expect that the stability of *Schlickgebiet* is (partially) maintained by the specific distribution of TKE and its dependence on the ROFIs.

5 Horizontal patterns of tidal asymmetry during neap and spring tides

As the tidal wave propagates into the estuary, nonlinearities associated with advection and friction caused by channel geometry and shallow depths in tidal flats distort the tides (Jay and Smith 1990), causing flood- or ebb-dominated conditions (Godin 1991). Flood dominance occurs when high-water tide propagates faster partially "catching up" with the previous low tide (Friedrichs 2010). The tidal asymmetry can

Fig. 7 Difference between turbulent kinetic energy simulated in CR and BR at the bottom layer during flood (2011/04/19/T01:00) (**a**), slack flood (2011/04/19T04:00) (**b**), ebb (2011/04/19/T07:00) (**c**) and slack ebb (2011/04/19T10:00) (**d**)
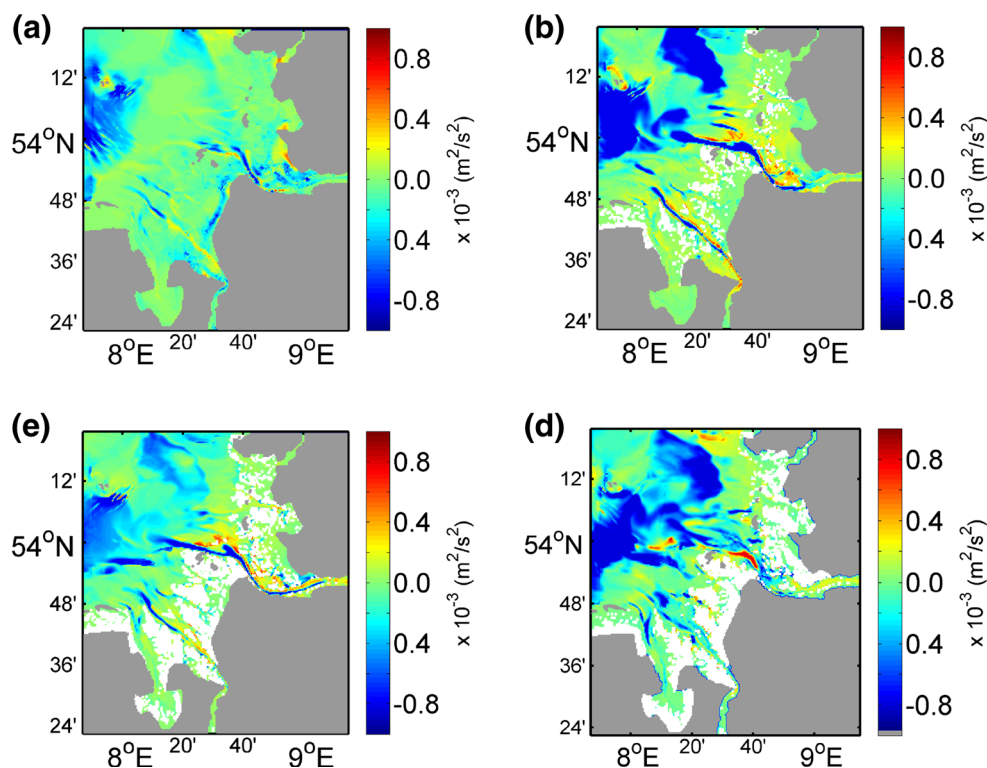
be examined by determining the length of flood and ebb period (flood-dominated asymmetry is characterized by a shorter flood time, while ebb dominance is characterized by a shorter ebb phase).

The asymmetries of tidal wave have been analysed earlier in the study area around Spiekeroog Island (Antia et al. 1996) and in the entire East Frisian Wadden Sea (Stanev et al. 2007b). Those results revealed the control by the hypsometry of intertidal basins and the dominant role of circulation caused by the tidally induced Stokes drift. Still missing from those studies was a description of the tidal asymmetry patterns in the corner of the German Bight (the south-east part of the bight) and beyond the barrier islands.

The ratio between the maximum flood and maximum ebb velocity magnitudes (v_{flood}/v_{ebb}) gave a reasonable representation of tidal asymmetries (Fig. 8). Areas where these values were larger than unity were flood dominated. Simulations using 1-km resolution revealed enhanced flood dominance in the bottom layer (compare Fig. 8a, b with Fig. 8c, d correspondingly). Another general finding was that the difference between the surface and bottom patterns was more pronounced during the neap than during the spring tide. This revealed the increased role of stratification during neap tide for the distortion of oscillations.

The horizontal patterns in Fig. 8a, b revealed low-value ratios oriented in the direction of the Elbe Valley. In the same area the bottom patterns (Fig. 8c, d) showed maxima. This gave an indication that in the Elbe Valley, the motion

was ebb dominated at the surface and flood dominated near the bottom. This pattern was better defined during the neap periods, when the stratification was strongest and was consistent with the development of gravitational circulation: fresh water outflow in the estuaries generates horizontal density gradients that drive the gravitational circulation with a net landward near-bed current. Thus, the change of the gravitational circulation from springs to neaps affected the tidal asymmetries.

The fine-resolution simulations although generally consistent with the results from the German Bight model added further details on the asymmetry patterns. From Fig. 8e–h, it became clear that the narrow channels and small-scale bathymetric features on the tidal flats dominated the small-scale structures in the tidal asymmetry. The flood dominance (ratios higher than unity) was observed on the tidal flats both at the surface and in the bottom layer. However, the most pronounced flood asymmetry was simulated in the bottom layer during neaps over most of the open-ocean part of model domain. During spring tide, this area reduced in size extending along the Elbe channel up to the Helgoland Island. The overall

Fig. 8 The ratio between the maximum flood and maximum ebb current ▶ speed (values larger than 1 indicate flood dominance). *Left* for the spring period (22 April 2011) and *right* for the neap period (28 April 2011). The figures on the *top* (**a–d**) are from the simulations in the entire German Bight; the ones *below* (**e–h**) are from the simulations with the fine-resolution estuarine model. Panels (a, b, e, f) are for the surface currents; (c, d, g, h) are for the bottom layer currents
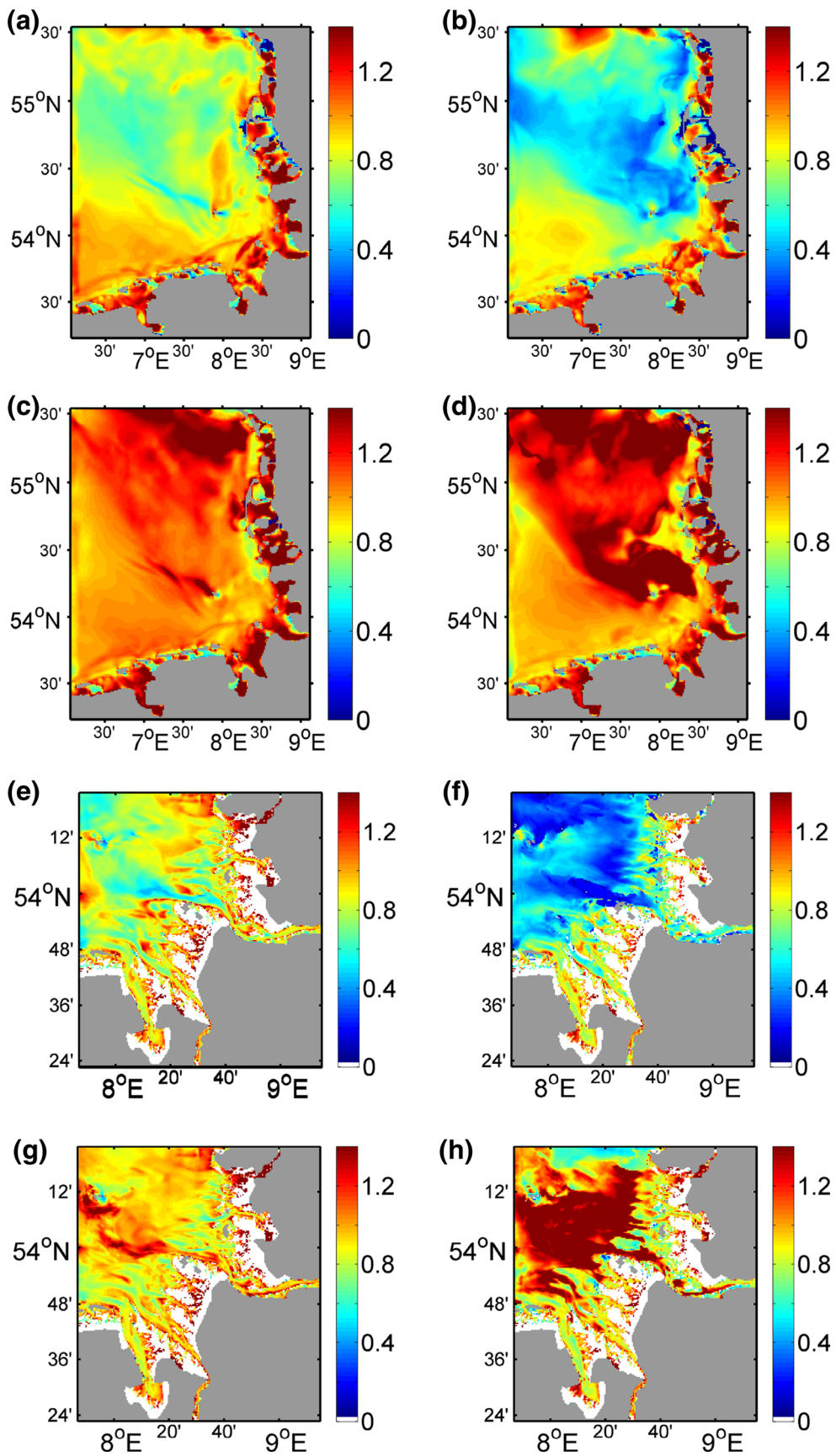
conclusion from the fine-model simulations is that in many cases, the ebb dominance at sea surface was accompanied by flood dominance in the bottom layer. This is associated with the so-called internal tidal asymmetry (Jay and Musiak 1996; Jay 2010), which is driven by correlations between tidal shear and vertical turbulent mixing. In nonhomogenous basins, the density stratification changes asymmetrically: during ebb the density contours are less vertical; during flood they are more vertical. This is called "tidal straining" (Simpson et al. 1990). The associated change in stratification is known as "strain-induced periodic stratification" or SIPS (Stacey et al. 1999). Additionally, different balances exist between the barotropic and baroclinic pressure gradients. The barotropic gradient changes its direction during the tidal cycle while the baroclinic is always directed from the sea to the coast. Thus, the two pressure gradient components oppose each other during ebb, resulting in an asymmetric evolution of the flow: more uniform flow on flood and a highly sheared ebb flow (see Figure 4.7 of Jay 2010).

The asymmetric responses were seen better for the neap tides than the spring tides. During the spring tide, the areas of surface ebb dominance and bottom flood dominance followed approximately the submarine part of the Elbe channel in the direction of the *Schlickgebiet* (see Fig. 1b). One could thus expect that this vertical separation of asymmetries explains (at least partially) the existence of large amount of fine sediment in this area. A trapping mechanism in this region seems plausible, which is supported by the export of fine fractions of sediment in the ebb direction and its deposition in the *Schlickgebiet*. At the *Schlickgebiet*, (1) the near-bottom is subject to flood-dominated asymmetry, which limits the export of sediment toward the open sea, and (2) the turbulence is reduced (see Section 4), which reduces resuspension. The above trapping mechanism works in parallel with the transport of SPM from the coastal zone along the major bathymetric channels, which ends in the area south of the Helgoland Island, i.e. in the *Schlickgebiet* (see Figs. 1b and 2b).

6 Vertical patterns of tidal flow asymmetry

6.1 Tidal distortion

The vertical structure of M_2, M_4 and M_6 major axes currents (Fig. 9) along the section line shown in Fig. 3 reveals the along-channel differences in the spectral composition of tides. This section line follows the submarine extensions of the Elbe Estuary, which is the main avenue for the exchange of water and matter between the tidal flats and the German Bight. The forthcoming analysis is instructive because it explains the three-dimensional exchange process. The magnitude of the M_2 major axis current (Fig. 9a) is an order of magnitude larger

than the M_4 and M_6 currents (compare with Fig. 9c, e). The M_2 pattern showed pronounced vertical shear that changed along estuary: weak and "diffuse" in the westernmost and easternmost parts of the section line and well-defined vertical shear in the middle of the channel. A maximum in M_2 currents is observed in the area north of Cuxhaven (at about km 43, see also Fig. 3) where the depth changed abruptly from 28 to 18 m.

The M_4 major axis current (Fig. 9c) displayed very different vertical structure in comparison to the M_2 current. Up to km 45, this constituent was <0.1 the M_2 amplitude. The M_4 major axis current increased just landward from the point where the M_2 current reached its maximum. This could indicate that the major transformation of the tide along the channel occurred north of Cuxhaven over a distance of ~10–20 km.

The vertical structure of the M_4 major axis current was very different from that of the M_2. The characteristic scales for the M_2 current were longer than the M_4 scales; the latter showed several minima west of km 40. A similar feature (smaller length scales in M_4 compared to M_2) was explained by Stanev et al. (2014) on the example of horizontal structure of M_2, M_4 and M_6 surface tidal currents.

The pattern of the M_6 major axis current was more similar to the M_2 than the M_4, which is explained by the fact that the M_6 is caused by nonlinear friction. Friction is exactly opposite to the currents, for which the largest constituent is the M_2. This issue was considered in more detail by Stanev et al. (2014) who demonstrated that the largest magnitudes of M_6 major axis surface current were located in the areas where the velocities were strongest and consequently where the friction was highest. However, two important differences between the distributions of M_2 and M_6 major axis currents can be mentioned: (1) the M_2 is surface intensified and (2) its magnitude decreases monotonically east of Cuxhaven. In contrast, the M_6 had a complex vertical structure with a maximum between surface and bottom. The basic conclusion from the above considerations is that (1) the tidal spectrum depends on bathymetry; however, (2) its appearance changes in the different parts of submarine channels.

The comparison between the results from the CR and BR, see left and right panels in Fig. 9, is indicative of the role of density stratification on tidal distortions. Although there are overall similarities between the results of the two experiments, several important differences are noteworthy. The comparison between the two experiments provides evidence that density stratification tends to decouple processes in the surface and bottom layers, enhancing thus the tidal amplitudes in the surface layers.

The vertical shear of tidal oscillations is smaller in the BR, while in the CR there is a marked surface intensification of the M_2 current. Also, baroclinicity favours a clear layered structure in the M_4 current and a sub-surface intensification of the M_6 current. The larger similarity between Fig. 9b and Fig. 9f

Fig. 9 Amplitudes of the major axes currents along the Elbe subsurface channel for spring tide. Three tidal constituents are presented: M_2 (**a**), M_4 (**c**), M_6 (**e**); (**b**, **d**, **f**) are the same but simulated in the barotropic experiment
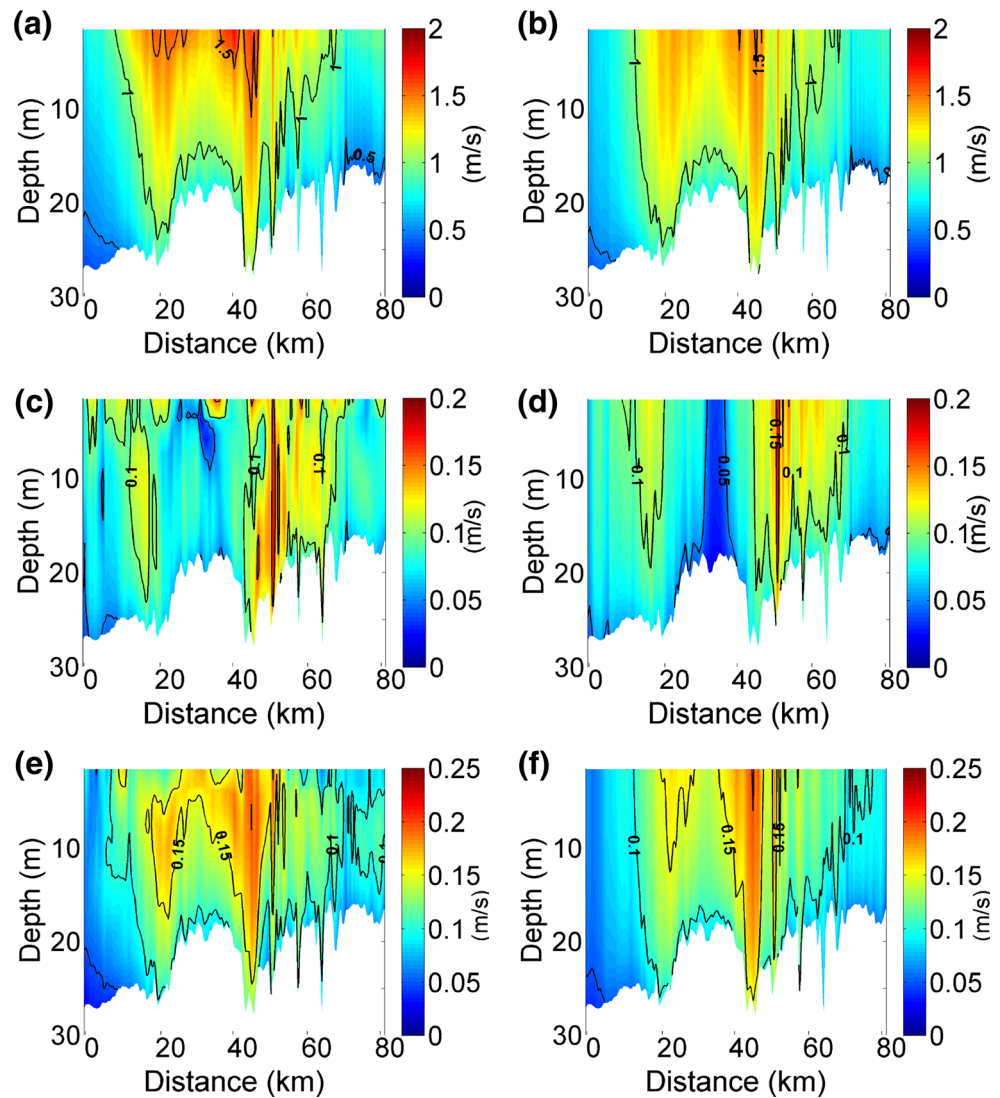
than between Fig. 9a and Fig. 9e demonstrated the tight connection between M_2 and M_6 under barotropic conditions. The differences between Fig. 9a and Fig. 9e are explained by the influence of density stratification. Another fundamental result is that the area between km 10 and 70 can be considered as the region of major distortions of tidal oscillations because of greatest M_2 tidal currents. The above results allow the expected conclusion that the river run-off can substantially affect tidal asymmetries and the resulting processes of material transport and sorting.

The ratios M_4/M_2 and M_6/M_2 are indicators of nonlinearities, which represent the effect of spectral energy transfer from M_2 to M_4 and M_6 (Speer 1984). The ratio of M_4 to M_2 major axes current displays three main areas (Fig. 10a): (1) the westernmost part (<20 km) where the tidal distortion was large, (2) the area between km 20 and 42 where the distortion was small and (3) the area east of km 42 where the M_4 magnitude was more than 10 % of the M_2. In this latter zone,

the tidal distortion was bottom intensified. These regional characteristics of M_4/M_2 distortion pattern identify the first zone as flood dominated. In the second zone, the ratio between M_2 and M_4 major axes current remained low until km 42 (north of Cuxhaven). East of this point the overtide became very important, in particular, in the bottom layer. This is approximately where the ETM is observed (see Fig. 1b for the position of ETM); thus, the tidal transformation there should be of utmost importance for sediment dynamics.

The comparison with the results from BR (Fig. 10b) gave an overall support of the above analysis: again the same three zones were clearly identified. However, the bottom enhancement of distortion in the eastern zone and the reduction of distortion at the surface in the intermediate zone did not appear in BR.

The pattern of M_6/M_2 (Fig. 10c) displayed a layered structure, as was the case with the M_4 distortion. However, there was no zonation in M_6/M_2 as there was with M_4/M_2. Instead,

Fig. 10 The ratio between spring-tide M_4 and M_2 amplitudes (a) and M_6 and M_2 amplitudes (c); (b and d) are the same but resulting from barotropic experiment
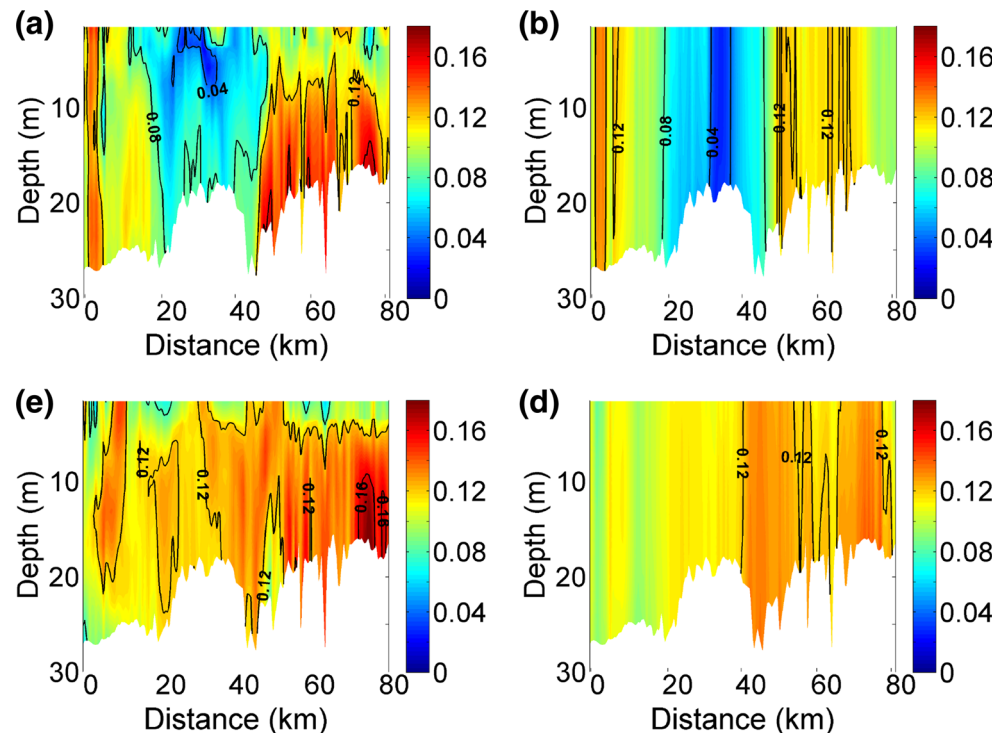
there was a continuous increase of M_6/M_2 ratio from east to west, with the largest distortion occurring where the ETM zone was usually observed (see Fig. 1b). It is noteworthy that the M_6/M_2 distortion had longer scales than the topographic scales. In other words, the M_6 generation could not be fully explained by the small-scale local topography (not every individual change of depth resulted in a change of spectral composition, Fig. 10b). Again, like in the M_4/M_2 case, the comparison between CR and BR simulations demonstrated a slight similarity along the estuary. However, the effect of fresh water flux appeared very important for the vertical structure of the tidal distortion.

7 Spring-neap changes in tidal asymmetry

The ratio of maximum flood to maximum ebb current gives an overall idea on patterns of tidal asymmetry. Values in Fig. 11 larger than unity indicate flood dominance; values smaller than unity indicate ebb dominance (Friedrichs and Aubrey 1988). The neap tide showed ebb dominance in the central parts of the channel. In both cases (neap and spring tide), flood dominance appeared in the westernmost part of the section (filling the whole water column, but more pronounced in the surface layers). However, the situation changed completely in the ETM zone where the bottom-intensified flood dominance was very pronounced during the spring tide. This was consistent with the overall comparison between neap and spring

tides, although spring tide patterns are more "shifted" toward flood dominance. Bearing in mind that tidal asymmetries determine the direction of net sediment transport (Postma 1961; Groen 1967; Friedrichs and Aubrey 1988) and the fact that there are multiple zones of opposite asymmetries along the Elbe bathymetric channel, one can conclude that these opposing asymmetries would support divergence or convergence of fluxes. Specific positions of convergence or divergence are strongly dependent on the phase of neap-spring variations.

Even more fundamental conclusions follow from the comparison between the results of BR and CR. The first one is that fresh water largely controls the ratios between the maximum flood and maximum ebb current speed, which is seen in the comparison between right and left panels of Fig. 11. The second conclusion is that the differences between neap and spring conditions are largely caused by fresh water. This follows from the fact that the differences between top and bottom rows of Fig. 11 are larger in the CR. Considering that the above ratios largely determine the sediment dynamics, it could be concluded that the neap-to-spring variability in sediment transport is largely dominated by river run-off and gravitational circulation, which are missing in the barotropic ocean.

Looking back to Fig. 4, one sees that the maximum tidal distortions occur approximately in the area of largest along-channel divergence and convergence of tidal currents. This is the same area where the maximum salinity gradient is also observed (Fig. 12). This gradient decreases by 20 % during spring tide. It is also seen in Fig. 4 that the estuary can be roughly considered as composed of three parts: outer estuary

Fig. 11 The ratio between the maximum flood and maximum ebb current speed during spring (**a**) and neap (**c**) tide; (**b** and **d**) are the same but from the barotropic experiment
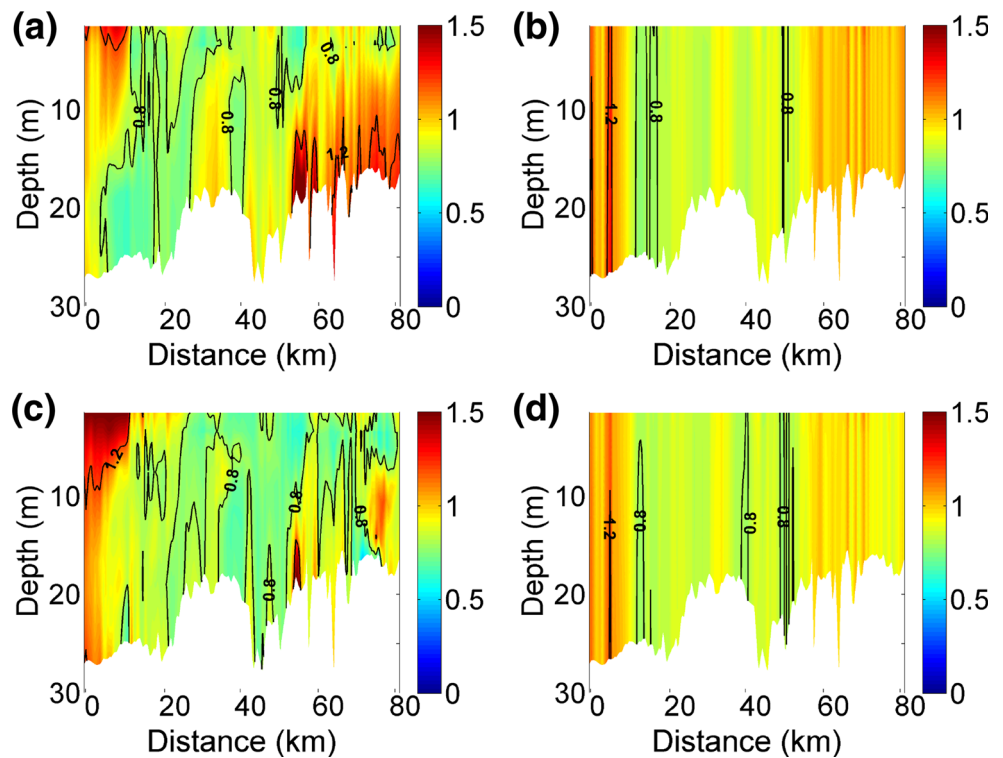
with salinities approaching 30 g/kg downstream of km 20, salinity-front area between km 20 and 55 and tidal river which is upstream of km 55. In the first area the salinity range is relatively small. In the second area characterized by large salinity gradients the estuarine circulation contribute to a substantial change of tidal wave properties. In the third area, the along-channel salinity gradient decreases again. The above characteristics of the along-estuary salinity field are consistent with those of other estuaries (e.g. see Monismith et al. 2002).

The along-channel density gradient has a central role in estuarine dynamics. It is not a coincidence that the

Fig. 12 Mean for the neap tide surface salinity gradient along the section line *A–B* (see Fig. 1b for the position)

nonlinearities and the resulting distortion in the tidal signal occur in the area of the salinity front. The along-channel density gradient determines the horizontal Richardson number known also as the Simpson number:

$$Si = \frac{b_x H^2}{C_D U_T^2},$$

where b_x is the along-channel derivative of buoyancy $b = -g(\rho - \rho_0)/\rho$, U_T is the amplitude of vertically averaged along-channel velocity (U), H is the depth and C_d is the friction coefficient. This nondimensional number reflects the competition between baroclinic and barotropic forcing (Stacey et al. 2010). At values of $Si > 0.15$, the estuary is partially mixed due to tidal straining. For $Si < 0.15$, the estuary is permanently mixed. In our case, that is, $Si < 4 \times 10^{-3}$ during all times, the estuary is very well mixed. During neap tide, Si is more than two times larger than during spring tide, which explains the sensitivity of the estuarine system to the combination between tidal forcing with different amplitudes and river run-off (see Fig. 11).
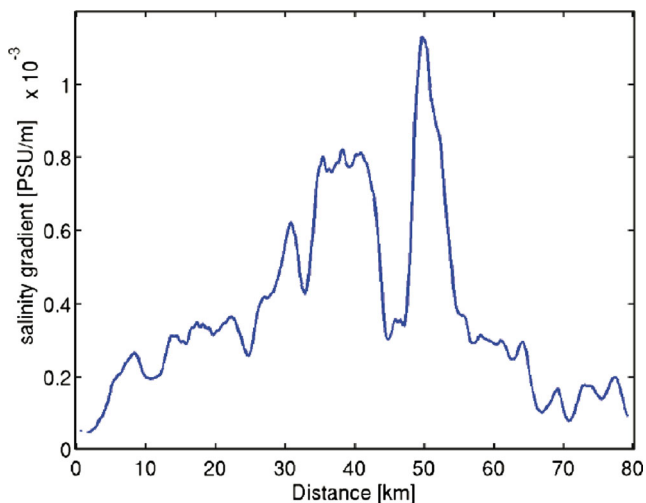
8 Discussion

The "competition" between the river outflow stabilizing the water column and tidal mixing in the region resulted in well-

mixed conditions over most of the model domain with different salinity gradients reaching a maximum north of Cuxhaven. The vertical shear of horizontal velocity displayed the well-known gravitational circulation patterns. The velocity shear was largest in the Elbe bathymetric channel, while the tidal oscillations had lower amplitudes in the Weser channel, in particular, in the bottom layer. It was demonstrated that the correlation between salinity and velocity tended to enhance the vertical overturning. The frontal areas were subject to complex dynamics shaped by the physical balances and bathymetry.

The front position and sharpness changed dramatically between flood and ebb tide. New elements in the regional processes were revealed on the basis of numerical simulations, such as the phase shift of currents along the channel. This resulted in the formation of divergent or convergent flows; the largest tidal excursions were associated with the maximum divergence/convergence of currents in the mouth (Fig. 4). This maximum appeared in the area of salinity front, shaping thus the exchange of water between the tidal channels and tidal flats. This result supports the hypothesis of Geyer and Signell (1992) and MacCready (2004) relating the horizontal mixing to the tidal excursion.

Important for the understanding of results presented here is the relationship between tidal excursion L_T and the amplitude of the tidal current U_T:

$$L_T = U_T T_T / \pi,$$

where T_T is the tidal period (MacCready 2004). The salinity front and the maximum of divergent/convergent flows (Fig. 4 and 12) appeared where the nonlinearity of dynamics exemplified in the present study by the tidal distortion was very pronounced. In this area L_T attained a maximum value. Therefore, estuarine theories should probably account for the joint contributions of nonlinearities and baroclinicity. The present research can be thus considered as an illustration of the interaction between the tidal flow and the density gradient in a region influenced by fresh water. This is of utmost importance because it can have broader applications for other coastal regions. In the tidal system considered here, the horizontal density gradient drives density currents which add to the tidal currents. The tidal straining, in which the shear in the tidal flow combines with the horizontal density gradients, affects the stability of the water column (Simpson et al. 1990). This couples barotropic and baroclinic processes, resulting thus in a distortion of tidal signal having a maximum in the area of the salinity front. The above conclusions complement the results of Nunes and Simpson (1985) and Simpson et al., 1990 (1990) who related the distance of penetration of a front with the river discharge and tidal range.

Sensitivity experiments carried out with and without fresh water fluxes from rivers contributed to quantifying the role of stratification for the regional estuarine dynamics. The numerical simulations supported the ideas linking the reduced production of TKE in stratified flows to decreasing the strength of turbulence. Because the bed shear stress changes from the CR simulation to the BR simulation, the comparison between the two simulations indicated possible variability of sediment dynamics caused by the water density field. The resulting trend was such that the channel TKE values of Elbe and Weser were less in the CR, suggesting that vertical stratification would decrease bottom erosion in the tidal channels. More important, however, was that in the CR the TKE, values were lower in the area of the *Schlickgebiet*, which demonstrated that the baroclinicity would enhance deposition and suppress the remobilization there. This has been considered as an explanation of sediment trapping in this region, demonstrating the role of ROFI for the near-bottom accumulation of sediment.

To the authors' knowledge, no deep consideration has been given in the past to the vertical patterns of tidal asymmetries and their possible role for material transport and deposition in the studied area. The amplitudes of the maximum axial currents and the ratios between the maximum flood and maximum ebb velocity gave a reasonable representation of regional tidal asymmetries. The numerical simulations supported theories and demonstrated enhanced flood dominance in the bottom layer and ebb dominance in the surface layers with a strong dependence upon the neap-spring cycle. The difference between the surface and bottom patterns of tidal asymmetry was more pronounced during the neap than during the spring tide, again stressing the role of stratification (larger during neap tide) for the distortion of tidal oscillations. These vertical patterns of tidal asymmetries could additionally validate the proposed trapping mechanism in the *Schlickgebiet* region. Validation comes from the export of fine fractions of sediment in the ebb direction and deposition where bottom flow is flood dominated, which limits the export of sediment toward the open sea. Admittedly, the area around the *Schlickgebiet* is not the one with the strongest flood dominance. Therefore, the results of Fig. 8 offer initial indications. Further understanding of these possible mechanisms can be achieved using a sediment model, which will be the subject of a separate study.

Another novel aspect of the tidal dynamics discussed in this paper was the tidal distortion quantified as the ratio between individual tidal constituents. The M_2 pattern showed pronounced vertical shear with along-estuary variability. One key area of tidal distortion was the regions north and east of Cuxhaven, which (1) was subject to pronounced divergences and convergences of the flow and (2) where the

salinity front was most pronounced. Exactly in this region, the M_4 major axis current started to increase landward. This could indicate that the major transformation of the tide along the channel occurred north of Cuxhaven over a distance of ~10–20 km. In this area of large dynamical complexity, density stratification decoupled surface from bottom processes. A complex structure of surface-enhanced and bottom-enhanced distortions occurred, which were quite different for M_4 and M_6 tides. East of Cuxhaven, the overtides increased in magnitude, in particular, in the bottom layer. This is approximately where the ETM is observed (Kappenberg and Fanger 2007) and where the model revealed strong tidal transformation, which are known to be of utmost importance for sediment dynamics. The Elbe bathymetric channel revealed multiple zones with opposite asymmetries. Their specific positions were strongly dependent on the phase of neap-spring variations. In the ETM zone, the bottom-intensified flood dominance was very pronounced during the spring tide, explaining the observed variability of SPM (Kappenberg et al. 1996).

9 Conclusions

The numerical simulations presented in this study detected the estuarine salinity front in the area north of Cuxhaven where the dominant physical balances and bathymetry resulted in a complex estuarine dynamics. The maximum divergence/convergence of currents and the largest tidal excursions occurred also in this part of the river mouth. These oscillations were exemplified by the increase of the amplitude of overtides identifying the role of the nonlinear dynamics in the same area. Furthermore, the correlation between salinity and velocity at intertidal time scales explained about 20 % of the vertical overturning. The complex structure of surface-enhanced and bottom-enhanced tidal distortions, which were different for M_4 and M_6 tides, demonstrated that the density stratification decoupled surface from bottom processes. The latter was clearly illustrated in the comparison between baroclinic and barotropic experiments demonstrating that density gradients affect the rates of nonlinear transformation of tidal signals. This motivates an extension of estuarine theories accounting for the joint contributions of nonlinearities and baroclinicity.

A demonstration has been given that the physical processes affecting the sediment dynamics were very sensitive to the water density providing an explanation of sediment trapping in some areas and the near-bottom accumulation of sediment there. These and other results could have more general implications for other estuarine areas because the dominant physical mechanisms are the same.

References

Antia E, Flemming B, Wefer G (1996) Patterns of tidal flow asymmetry on shoreface-connected ridge topography off Spiekeroog Island, German bight. Ger J Hydrogr 48:97–107

Backhaus JO (1980) Simulation von Bewegungsvorgängen in der Deutschen Bucht. Dt Hydrogr Z Erg H B 15:56 pp

Burchard H, Bolding K (2002) GETM – a general estuarine transport model. Scientific documentation, no EUR 20253 EN, European Commission, printed in Italy. 157 pp

Carbajal N, Pohlmann T (2004) Comparison between measured and calculated tidal ellipses in the German Bight. Ocean Dyn 54:520–530

Egbert G, Erofeeva S (2002) Efficient inverse modeling of barotropic ocean tides. J Atmos Ocean Technol 19(2):183–204

Figge K (1981) Sedimentverteilung in der Deutschen Bucht. Karte Nr. 2900 mit Beiheft. Deutsches Hydrografisches Institut

Friedrichs CT (2010) Barotropic tides in channelized estuaries. In: Valle-Levinson A (ed) Contemporary issues in estuarine physics. Cambridge University Press, Cambridge, pp 27–61

Friedrichs CT, Aubrey DG (1988) Non-linear tidal distortion in shallow well mixed estuaries: a synthesis. Estuar Coast Shelf Sci 27:521–545

Geyer WER, MacCready P (2014) The estuarine circulation. Annu Rev Fluid Mech 46:175–97

Geyer W, Signell R (1992) A reassessment of the role of tidal dispersion in estuaries. Estuaries 15(2):97–108

Godin G (1991) Frictional effects in river tides. In: Parker BB (ed) Tidal hydrodynamics. Wiley, New York, pp 379–402

Groen P (1967) On the residual transport of suspended matter by an alternating tidal current. Neth J Sea Res 3(4):564–574

Hansen DV, Rattray M (1966) New dimensions in estuary classification. Limnol Oceanogr 11:319–326

Jay DA (2010) Estuarine variability. In A. Valle-Levinson (Ed.), Contemporary issues in estuarine physics, pp. 62–99

Jay DA, Musiak JD (1996) Internal tidal asymmetry in channel flows: origins and consequences. In C. Pattiaratchi (ed.), Mixing processes in estuaries and coastal seas, an American Geophysical Union Coastal and Estuarine Sciences Monograph, pp. 219–258

Jay DA, Smith JD (1990) Circulation, density distribution and neap-spring transitions in the Columbia river estuary. Prog Oceanogr 25:81–112

Kappenberg J, Fanger H-U (2007) Sedimenttransportgeschehen in der tidebeeinflussten Elbe, der Deutschen Bucht und in der Nordsee. Gutachten GKSS 2007/20 des GKSS Forschungszentrums, Geesthacht GmbH, im Auftrag von Hamburg Port Authority. 125 pp

Kappenberg J, Grabemann I (2001) Variability of the mixing zones and estuarine turbidity maxima in the Elbe and Weser estuaries. Estuaries 24:699–706

Kappenberg J, Schymura G, Kuhn H, Fanger H-U (1996) Spring/neap variations of suspended matter concentration and transport in the turbidity maximum of the Elbe Estuary. Advances in Limnology, 47,

Particulate Matter in Rivers and Estuaries, Archiv für Hydrobiologie, S. 323–332

MacCready P (2004) Toward a unified theory of tidally-averaged estuarine salinity structure. Estuaries 27(4):561–570

Mayer B (1995) Ein dreidimensionales, numerisches schwebstoff-transportmodell mit anwendung auf die Deutsche Bucht. Tech. Rep. GKSS 95/E/59, GKSS-Forschungszentrum Geesthacht GmbH

Monismith SG, Kimmerer W, Stacey MT, Burau JR (2002) Structure and flow-induced variability of the subtidal salinity field in northern San Francisco Bay. J Phys Ocean 32(11):3003–3019

Nunes RA, Simpson JH (1985) Axial convergence in a well-mixed estuary. Estuar Coast Shelf Sci 20:637–49

Pawlowicz R, Beardsley B, Lentz S (2002) Classical tidal harmonic analysis including error estimates in MATLAB using T_TIDE. Comput Geosci 28:929–937

Postma H (1961) Transport and accumulation of suspended matter in the Dutch Wadden Sea. Neth J Sea Res 1:148–190

Ridderinkhof S (1997) The effect of tidal asymmetries on the net transport of sediments in the Ems Dollard estuary. J Coast Res 25:41–48

Rolinski S, Eichweber G (2000) Deformations of the tidal wave in the Elbe estuary and their effect on suspended particulate matter dynamics. Phys Chem Earth (B) 25(4):355–358

Staneva J, Stanev E, Wolff J, Badewien T, Reuter R, Flemming B, Bartholom€a A, Bolding K (2009) Hydrodynamics and sediment dynamics in the German Bight. A focus on observations and numerical modelling in the East Frisian Wadden Sea. Cont Shelf Res 29(1):302–319. doi:10.1016/j.csr.2008.01.006

Sager G (1968) Atlast der Elemente des Tiedenhubes und der Gezeitenströme für die Nordsee, den Kanal und die Irische See. 2 Aufl IX, 58S. Rostok: Seehydrographischer Dienst, DDR

Simpson JH, Nunes RA (1981) The tidal intrusion front: an estuarine convergence zone. Estuar Coast Shelf Sci 13:257–266

Simpson JH, Brown J, Matthews J, Allen G (1990) Tidal straining, density currents, and stirring in the control of estuarine stratification. Estuaries 13(2):125–132

Speer PE (1984) Tidal distortion in shallow estuaries. PhD. thesis, 924 WHOI-MIT Joint Program in Oceanography, Woods Hole, MA, 210 pp

Stacey MS, Monismith G, Burau J (1999) Observations of turbulence in a partially stratified estuary. J Phys Oceanogr 29: 1950–1970

Stacey MT, Brennan ML, Burau JR, Monismith SG (2010) The tidally averaged momentum balance in a partially and periodically stratified estuary. J Phys Oceanogr 40:2418–2434

Stanev EV, Floeser G, Wolff J-O (2003) First- and higher-order dynamical controls on water exchanges between tidal basins and the open ocean. A case study for the East Frisian Wadden Sea. Ocean Dyn 53: 146–165

Stanev EV, Brink-Spalink G, Wolff J-O (2007a) Sediment dynamics in tidally dominated environments controlled by transport and turbulence: a case study for the East Frisian Wadden Sea. J Geophys Res 112:C04018. doi:10.1029/2005JC003045

Stanev EV, Flemming BW, Bartholomä A, Staneva JV, Wolff J-O (2007b) Vertical circulation in shallow tidal inlets and back-barrier basins. Cont Shelf Res 27:798–831

Stanev EV, Schulz-Stellenfleth J, Staneva J, Grayek S, Seemann J, Petersen W (2011) Coastal observing and forecasting system for the German Bight—estimates of hydrophysical states. Ocean Sci 7: 569–583

Stanev ES, AlNadhairi R, Staneva J, Schulz-Stellenfleth J, Valle-Levinson A (2014) Tidal wave transformations in the German Bight. Ocean Dyn 64:951–968

Valle-Levinson A (ed) (2010) Contemporary issues in estuarine physics. Cambridge University Press, Cambridge, p 315

Valle-Levinson A (2011) Classification of estuarine circulation. In: Wolanski E, McLusky DS (eds) Treatise on estuarine and coastal science, vol 1. Academic, Waltham, pp 75–86

van de Kreeke J, Robaczewska K (1993) Tide-induced residual transport of coarse sediment; application to the Ems Estuary. Neth J Sea Res 31(3):209–220

van Haren H (2003) Current spectra under varying stratification conditions in the central North Sea. J Sea Res 51(2004):77–91

van Leeuwen SM, de Swart HE (2002) Intermediate modeling of tidal inlet: spatial asymmetries in flow and mean sediment transport. Cont Shelf Res 22:1795–1810

von Haugwitz W, Wong HK, Salge U (1988) The Mud Area southeast of Helgoland: a reflection seismic study. In: Kempe, S.; Liebezeit, G.; Dethlefsen, V.; Harms, U. (Eds.): Biogeochemistry and distribution of suspended matter in the North Sea and implications for fisheries biology. SCOPE/UNEP Sonderband, Mitt. Geol.-Paläontolog. Inst. Univ. Hamburg, 65, S. 409–422

Winter C (2011) Macro scale morphodynamics of the German North Sea coast. J Coast Res SI 57:706–710